NANOSYSTEMS: PHYSICS, CHEMISTRY, MATHEMATICS, 2019, 10 (4), P. 456–465

Preparation and properties of CeO_2 sols stabilized by polyvinyl alcohol

S. A. Kuznetsova, A. A. Gordeev, D. A. Fedorishin, V. V. Kozik

Department of Chemistry, Tomsk State University, Tomsk, Siberia, Russia

onm@chem.tsu.ru, gaa1998sukh-mo@mail.ru, strix187@yandex.ru, vkozik@mail.ru

PACS 82.70.Gg **DOI 10.17586/2220-8054-2019-10-4-456-465**

The CeO_2 sols stabilized by polyvinyl alcohol (PVA) were obtained from solution of cerium nitrate (III) in the presence of hydrogen peroxide and ammonia. X-ray diffraction, transmission electron microscopy, the pH metric method, ultraviolet spectroscopy and infrared spectroscopy were used to investigate the compositions and properties of the sols. It was observed that the PVA stabilizes the colloidal solution of cerium dioxide. The stability of the solution depends on the mass content of PVA and pH. The surface of various CeO_2 particles exhibiting the property of an acceptor interacts with OH groups of PVA. CeO_2 sol with 5 wt.% PVA and pH 8.55 (particle size 67 nm) has sun protection properties (UVA/UVB = 0.64) and is characterized by low photocatalytic activity, cytotoxicity and genotoxicity.

Keywords: cerium dioxide sol,sun protection properties, methyl orange, propertiesof sol, polyvinyl alcohol.

Received: 18 July 2019

Revised: 4 August 2019

1. Introduction

Ultraviolet radiation is very important in human life. UV rays have exhibitedanalgesic and sedative effects. Strictly metered-dose UV irradiation stimulates the production of antibodies, thus increasing the resistance of humans to infection.Despite its important role in medicine, the harm of ultraviolet radiation on health exceeds the benefits. The ultraviolet range of the spectrum is conventionally divided into several regions. The most dangerous region of UV-radiation is UV-B radiation with wavelengths ranging from 290 to 320 nm [1]. The long-term effects of UV B on human skin can cause the incidence of skin cancer, including cutaneous melanoma, and photo aging of the skin [2]. Currently, inorganic UV filters based on ZnO and TiO_2 are widely used to protect the skin from well-known carcinogenic effects of ultraviolet light in cosmetic creams, including sunscreen. However, these metal oxides also have some disadvantages; numerous studies have shown that titanium and zinc oxide nanoparticles have high photocatalytic activity [8–10]. The authors of the work [11] showed that titanium dioxide is a photocytotoxic substance to the fibrous region of the skin. Analysis of the literature shows that approximately 20 years ago researchers proposed to use cerium dioxide as an inorganic UV filter [12–14]. This oxide over titanium and zinc oxides has several advantages, among which it should be noted a yellowish color of the substance (close to the skin color), transparency in the visible region of the spectrum, the ability to effectively absorb UV radiation [15,16], decrease in photocatalytic activity with decrease in particle size [17]. Information about CeO_2 photocatalytic activity which provided in the literature is ambiguous. It is believed that CeO_2 has a low photoactivity due to the large band gap (3.19 eV) and rapid recombination of photogenerated charge carriers. Photocatalytic activity is increased due to the addition of metal additives [18] or metal oxides [19–21] in cerium dioxide. The authors of [22] found that CeO_2 nanoparticles reduce oxidative DNA damage caused by UV irradiation. Other authors indicate that cerium dioxide exhibits photocatalytic properties [23–26]. The comparative analysis of literature indicates that state of the oxide surface and the presence of defects [25,26] and Ce^{3+} state [27] in the composition of oxide affect its photocatalytic properties and depend on conditions of its preparation.

Despite the large number of known synthetic methods, today there is an open question related to the development of new methods of producing of CeO_2 sol, which take into account the possibility of high-quality purification from reaction by-products and unreacted substances. Also, important task is searching a new non-toxic stabilizers, allowing obtaining stable sols with biologically relevant pH values. Polyvinyl alcohol (PVA) can be used as such a non-toxic stabilizer, which forms adsorption layers on the surface of dispersed particles and contributes to Van der Waals London interactions. It is known [28, 29] that PVA is usually weakly charged at neutral pH and therefore the stabilization of nanoparticles in the sol is due to electrostatic repulsion.

The aim of this study is obtaining sol of CeO_2 with PVA from cerium (III) nitrate solution and investigating photocatalytic, toxic and sunscreen properties of sol.

2. Experimental procedure

2.1. Materials

Cerium nitrate (III) hexahydrate (purity 99.9 wt.%) was purchased from Novosibirsk plant of rare metals. PVA-16/1 was purchased from company "Nevinnomyssky Azot". The solution of ammonia (25 wt.%) and the solution of hydrogen peroxide (30 wt.%) were purchased in the JSC "Base No. 1". Distilled water was used throughout the experiments. Methyl orange (MO) was purchased from Alfa Aesar.

2.2. Synthesis of CeO_2 sols

Procedure for preparing of light yellow and transparent CeO_2 sols is as follows. The aqueous solution of PVA (5 wt.%) was added to the solution of $Ce(NO_3)_3$ (C = 0.001 M) in a 1:5 volume ratio under magnetic stirring (3 K/min). The aqueous solution of H_2O_2 (30 wt.%) was then added to form a red color of $Ce(OH)_3OOH$. This solution was heated to 90 °C with constant stirring for 45 minutes. The aqueous solution of ammonia (0.03 – 1.5 ml 24 wt.%) was then added and left to mix at 90 °C for more 3 hours. Finally, prepared sol was allowed to air cool. The formation of cerium dioxide can be represented by the following reaction equation:

$$2Ce(NO_3)_3 + H_2O_2 + 6NH_3 \cdot H_2O = 2CeO_2 + 6NH_4NO_3 + 4H_2O.$$

The particles of cerium dioxide in the solid phase were obtained by the same method, using 2 wt.% solution of PVA and 0.5 ml solution of ammonia 24 wt.%. After several hours in such light yellow and transparent CeO_2 sol, the oxide particles coagulate and precipitate. The precipitate was filtered, washed with distilled water and dried at room temperature.

2.3. Characterization methods the composition and properties of sols

X-ray diffractograms (XRD) of solid samples (CeO_2) were recorded on a Rigaku Miniflex 600 powder diffractometer (CuKα emission) at a voltage, and current of 40 kV and 15 mA, respectively. The range $2\theta = 10\ ^\circ - 90\ ^\circ$ at a rate of 2 $^\circ$min^{-1} was used to identify the crystalline structure. The samples' phase compositions werefound using the ICSD PDF-2 database. The average crystallite size was calculated from the XRD peak (111) using the Scherer equation: $L = \dfrac{0.9\lambda}{\beta \cos\theta}$. High-resolution images and selected area electron diffraction (SAED) patterns were observed with a JEOL JEM-2100F transmission electron microscope (TEM) operating at 200 kV. The acid–base properties of the CeO_2 surface were studied using a Multitest pH meter by a procedure described in work [30]. The change pH of the cerium dioxide suspension in bidistilled water over time from the moment of formation until reaching the electrochemical equilibrium was detected according to the pH meter readings with the combined glass electrode ESC-10605. IR spectra of PVA, sols of CeO_2 with PVA and dried at 90 °C sols of CeO_2 with PVA were measured on an Agilent Cary 630 FTIR spectrophotometerin the frequency range 400 – 4000 cm^{-1}. The absorption and transmission spectra of sols in the visible region in ultraviolet were removed relative to the aqueous solution of PVA and relative to air (PE-5400 UF spectrophotometer). The average size of cerium dioxide particles in the sol was determined by the "turbidity spectrum" method. The method is based on the use of the Rayleigh equation for colloidal systems with low concentration, the dispersed phase of which does not absorb incident light and is optically isotropic [31].

The photocatalytic activity was evaluated for the decomposition of MO (as a model reaction) under UV light irradiation. For this, we used samples of the dried CeO_2 sol with PVA, as well as samples of CeO_2 particles without PVA, which were separated from the sol with higher oxide content. The 42 ml solution of MO (concentration of 12.760 g/l) and 0.425 g of the sample were placed into a reactor of quartz glass. The mixture was kept in the dark under magnetic stirring for 1 h to reach sorption–desorption equilibrium. Next, the reaction mixture was placed under an I_2 excimer ultraviolet lamp with $\lambda = 342$ nm and exposed to UV radiation for 1 h with constant stirring. Every 10 min, we took an aliquot, which was centrifuged to separate the precipitate, and then the absorbance of the mother liquor was measured. The methyl orange concentration was determined spectrophotometry method on a PE-5400 UF spectrophotometer (cuvette length 10 mm, filming step 1 nm). The wavelength for the measurement was 461 nm, which is the maximum characterized adsorption wavelength of MO. The absolute accuracy limit in the transmission measurement was ± 0.5 %.

In this paper, we performed an analysis of the sun protection characteristics of cerium dioxide sols on middle (UVB) and near (UVA) UV ranges. To assess the effectiveness of skin protection in the UVB range, the UVA/UVB ratio was determined according to [32]:

$$\frac{\text{UVA}}{\text{UVB}} = \frac{\int_{320}^{400} \lg\left(\frac{1}{T(\lambda)}\right) d\lambda / \int_{320}^{400} d\lambda}{\int_{290}^{320} \lg\left(\frac{1}{T(\lambda)}\right) d\lambda / \int_{290}^{320} d\lambda}.$$

TABLE 1. Properties of sols CeO_2 with PVA 5 wt. %

V NH_3 initial, ml	pH value	Particle size, nm	Aggregative stability
0.03	8.11	—	—
0.10	8.31	60	+
0.30	8.46	63	+
0.50	8.55	67	+
1.50	9.49	68	—

The UVA/UVB value is the ratio of the mean absorption in the near and middle UV ranges. The efficiency of the photoprotective action of sol in the UVA range was estimated in units of the critical absorption wavelength [33]:

$$\int_{290}^{c} \lg\left(\frac{1}{T(\lambda)}\right) d\lambda = 0.9 \int_{290}^{400} \lg\left(\frac{1}{T(\lambda)}\right) d\lambda.$$

The study of the sun protection properties of sol was carried out by the method of experimental model of ultraviolet erythema in rats according to the guidelines for preclinical studies of drugs [34]. Male rats (Rattusnorvegicus forma alba) of the Wistar line with an average weight of 250 ± 25 g ($n = 5$) were used as a test system. All rats were divided into two groups – experimental and control. An object of study in the form of an ointment was applied to the hairless area of the skin on the abdomen of animals of the experimental group. On a similar area of the skin of animals of the control group was applied only ointment base c PVA. Acute erythema in experimental animals was caused by irradiation with UV rays of these skin areas at a dose of 1 MED (minimum erythemic dose) [35]. Animals during experimental were under combined etheric-xylazine anesthesia. A laboratory source of ultraviolet radiation with a power of 250 W with a natural ratio of UVA and UVB radiation intensities was used. The irradiated areas were exposed for 10 minutes. The severity of erythema and edema of the skin was assessed visually immediately, after 0.5; 1; 2 and 3 hours, as well as the next day after irradiation on a conditional 4-point scale. The values of scale were: 0 – no erythema, 1 – very weak erythema, 2 – weak erythema, 3 – moderate erythema, 4 – clearly expressed erythema [36].

Genotoxicity of CeO_2 sols with PVA was investigated using Allium cepa test [37]. This technique is based on the influence of the environment on the growth of the roots of Allium cepa bulbs. For the experiment sol of CeO_2 with PVA (prototype), solution of PVA (placebo) and H_2O distilled (control sample) were used. Sol was diluted with water in a ratio of 1:49. The PVA solution was also diluted. Experiments were duplicated 4 times. Bulbs were sprouted for three days while kept at room temperature. On the 4th day the bulbs were taken out. The length of the roots was measured. After that they were fixed with a clamp Clark. For microscopic examination the crushed cytogenetic preparations were prepared by the standard method. The toxic effect was determined by the length of the roots.

The cytotoxicity of the CeO_2sol with PVA was assessed on monocytes isolated from whole blood of a healthy person by magnetic separation using MTT test [38]. CeO_2 tablets of the test substances are poured in to 2 ml of cell suspension and allowed to incubate for 144 hours at 37 °C and 5 % CO_2. For the test, a 96-well plate was used. After 144-hour incubation of monocytes with test substances, 100 μl of cell culture suspension was placed in each well. Before the transfer of cells from the culture cup to the 96-well plate for the MTT test, the cell suspension was re-suspended. Then, 10 μl of MTT working solution was introduced into each well and incubated for another 3 hours in a CO_2 incubator with 5 % CO_2. After 3 hours, the tablet was removed from the CO_2 incubator and the medium in each well was replaced with a DMSO solution. After that, using a tablet reader Tecan Infinite F50, the optical density of each well was determined at 490 nm, and the measured background absorption at 620 nm was subtracted.

3. Results and discussion

3.1. Characteristics sols CeO_2 with PVA

It was found that the stability of sols is influenced by the amount of PVA and the pH value of sols, which is determined by the volume of ammonia. The sols of CeO_2 with PVA up to 5 wt.% and values pH of 8 – 11 are not formed. The oxide particles coagulate in the process of obtaining sols. The stability of CeO_2 sols with 5 wt.% PVA depends on pH values. Some properties of sols and their stability are summarized in Table 1.

The as-prepared sols were light-yellow and transparent. The pH values of the stable sols were slightly basic. The average size of the colloidal particles in such sols was characterized by comparable values. The average colloidal particle size in the filtered sol with pHvalue of 9.49 was 68 nm. Consequently, an increase in the particle size of more than 70 nm in the studied solutions leads to their coagulation. The morphology of the CeO_2 nanocomposites of sols with pH = 8.31 and pH = 8.55 was investigated by the TEM analysis, which is shown in Fig. 1(a, b). Fig. 1 shows that the CeO_2 nanoparticles don't have a pronounced cut and are agglomerated, regardless of the pH of the sols. The degree of agglomeration tends to decrease with increasing of pH sols. Electron diffraction data additionally indicate the polycrystalline nature of nanocomposites. The particle size of CeO_2 in sol with pH = 8.31 is in the range of 2 nm to 4 nm with a narrow particle size distribution. For a sol with pH = 8.55, the size of CeO_2 nanoparticles reaches from 4 nm to 10 nm and particles have a more regular spherical shape.

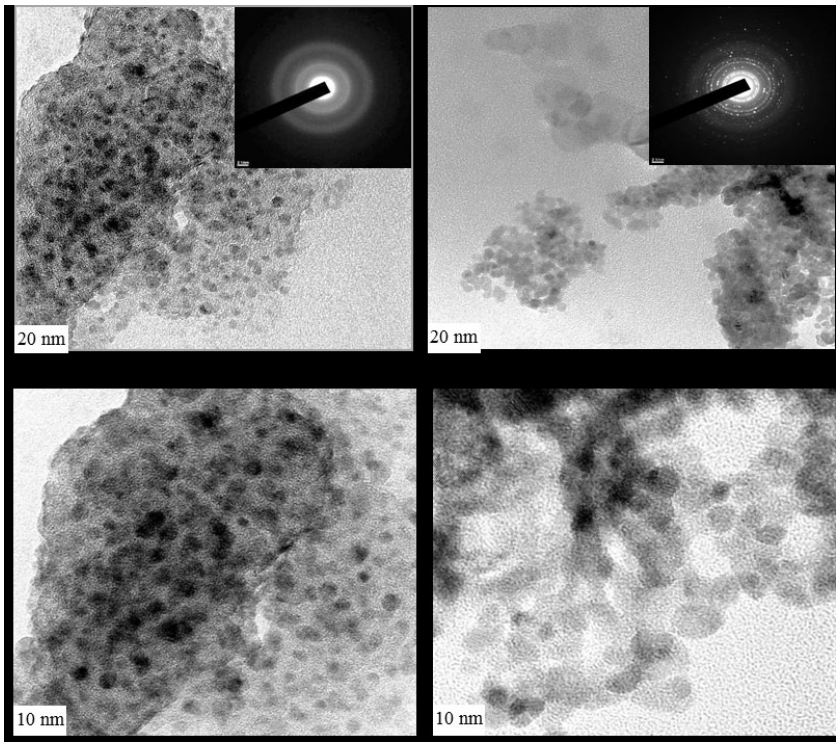

FIG. 1. TEM images of CeO_2 nanoparticles in sols with pH = 8.31 (a) and pH = 8.55 (b)

It is known [39,40], that the sun protection properties increase with increasing the size of particles in the sol. The sol with pH = 8.55 was stable and has a maximum particle size. This sol was investigated in this work.

Figure 2(a) shows the diffraction pattern of CeO_2 particle prepared from sol with PVA 2 wt.%. Diffraction peaks at $2\theta = 28.54352$, 33.09498, 47.46177, 56.349266, 59.089647, 69.44741, 76.61854, 79.03574 and 88.37222° correspond to the cubic phase (111), (200), (220), (311), (222), (400) (331) (420) and (422) cerium dioxide (from JCPDS card 00-034-0394).

The average crystallite size is 12.81 nm. Fig. 2(b) shows the diffraction pattern of the dried at 60 °C sol CeO_2 with PVA5 wt.%. (pH = 8.55). This sample contains a lot of amorphous phase. Diffraction peaks are wide and weak. The average crystallite size is 2.07 nm and is comparable with the value of nanocrystallites in sols (TEM).

The analysis of the IR spectra of solid PVA, PVA in an aqueous solution, sol of CeO_2 with PVA and dried at 60 °C sol of CeO_2 with PVA was performed to understand the interaction between CeO_2 and PVA in the sol. Fig. 3(a) shows absorption bands are observed at frequencies characterizing valent O–H bond vibrations (3400 – 3200 cm^{-1}) and C–H bond (2905 cm^{-1}) in the IR spectrum of solid PVA. A wide band of vibrations of O–H bonds indicates the formation of various associates in the solid phase of PVA [41].

The region of vibrations below the frequency of 1500 cm^{-1} corresponds to the valent vibrations of C–O group (1239 cm^{-1}), deformation vibrations of O–H groups (1140 cm^{-1}, 1081 cm^{-1}) and $–CH_2–$ groups of various types: scissors (1414 cm^{-1}); fan and torsion (915 cm^{-1}, 838 cm^{-1} syndio- and isotactic PVA structures, respectively [42] (Fig. 4).

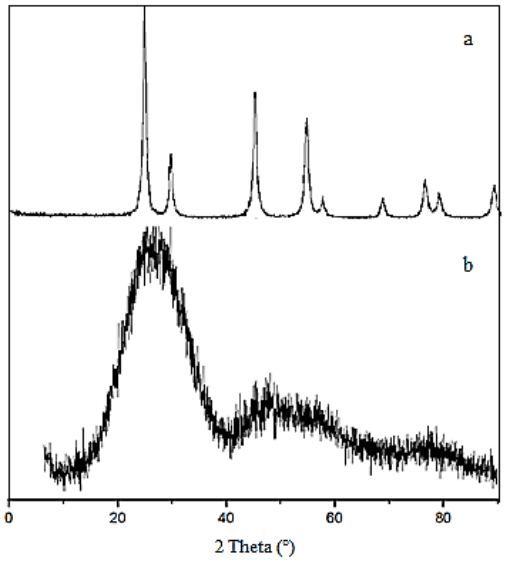

FIG. 2. XRD patterns of coagulated particles CeO_2 (a) and dried sol CeO_2 with PVA (b)

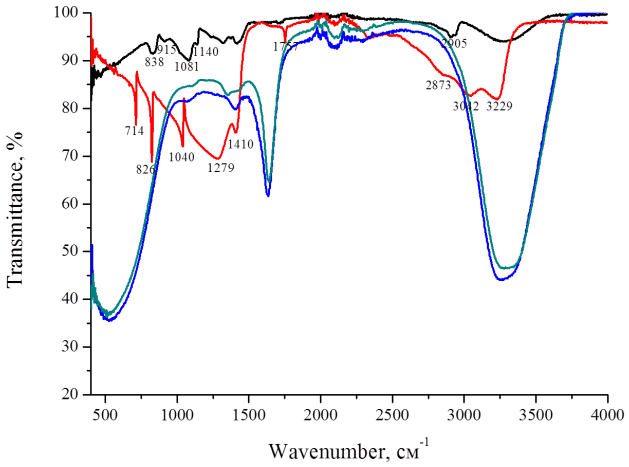

FIG. 3. IR spectra of solid PVA (a —), dried at 60 °C sol of CeO_2 with PVA (b —) PVA in an aqueous solution (c —) and sol of CeO_2 with PVA (d —)

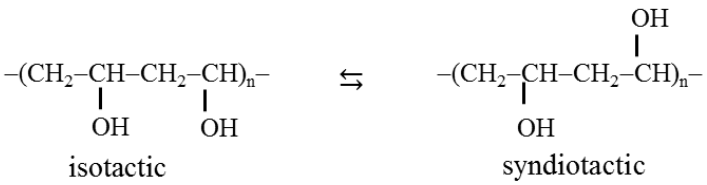

FIG. 4. Structure of the PVA

The frequencies of valent vibration of O–H groups (3042 and 3229 cm^{-1}), C–H group (2873 cm^{-1}), C–O group (1279 cm^{-1}) and deformation vibration of the O–H group (1040 cm^{-1}), $–CH_2$-group of an isotactic structure PVA (826 cm^{-1}) are also observed in the infrared spectrum of the dried sol of CeO_2 with PVA (Fig. 3(b)). In addition, in the IR spectrum of this sample there is apeak at frequency 714 cm^{-1}, which correspond to the deformation vibrations of the $–CH_2–$ group pendulum type. Proof of the interaction of CeO_2 with PVA is a change in the intensity of the observed absorption bands of valent and deformation vibrations and a shift of their wavelengths to the low-frequency region compared to the IR spectrum of PVA without CeO_2, as well as a shift in equilibrium towards the formation of the syndiotactic structure of PVA. The IR spectra of an aqueous solution of PVA and sol of CeO_2 with PVA are less informative because of the very wide absorption bands (Fig. 3(c, d)). However, when comparing them, a difference is also observed, especially in the region of vibrations of $–CH_2–$ groups.

The properties of the surface of CeO_2 were evaluated by the pH-metry method. The samples of CeO_2 obtained from sol with PVA 5 wt.% (pH = 8.11) were placed in bidistilled water and pH values of suspension over time were measured with constant stirring. Fig. 5 shows sharp decrease in pH of an aqueous suspension of CeO_2 to 3.95 during the first 60 seconds.

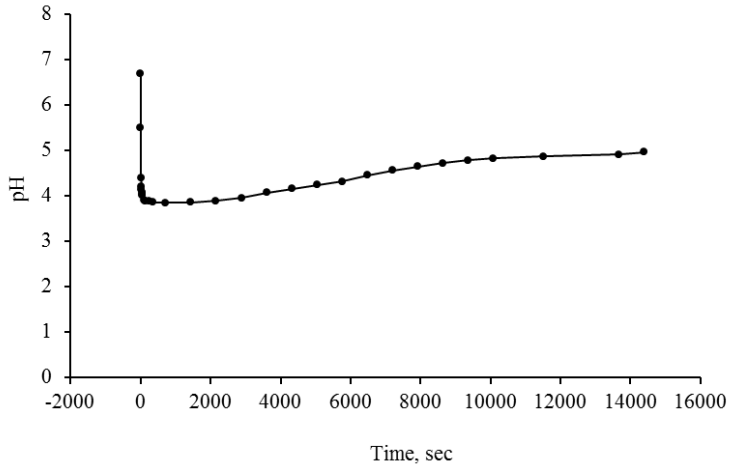

FIG. 5. Changes inpH of CeO_2 suspension over time

Such a change in pH indicates that the process of desorption of adsorbed water molecules from air from the surface of cerium oxide proceeds by the reaction:

$$\mathrm{CeO_{2-x}} \cdot y\mathrm{H_2O_{abs}} \leftrightarrows \mathrm{CeO_{2-x}} \cdot y\mathrm{OH^-} + y\mathrm{H^+}.$$

Changing the pH of the aqueous suspension of CeO_2 after 60 seconds isdue to the interaction with the surface of the CeO_2 liquid water by dissociation mechanism. Equilibrium in the reaction of water dissociation on the surface of CeO_2 occurs at pH = 4.96:

$$\mathrm{CeO_{2-x}} + z\mathrm{H_2O_{liq.}} \leftrightarrows \mathrm{CeO_{2-x}} \cdot z\mathrm{OH^-} + z\mathrm{H^+}.$$

Consequently CeO_2 is Lewis acid and can hold PVA with donor pairs of OH-group electrons. It is known [43], that part of the oxygen atoms on the surface of CeO_2 are absent in the corresponding crystallographic positions. Oxygen vacancies are formed, the effective degree of oxidation on the cerium atoms decreases to $+3$, and the cerium atoms can exhibit acceptor properties.

Figure 6 shows that in the UV spectrum of sol CeO_2 with PVA there are two broad absorption maxima at 305 and 275 nm, which characterize the content in the oxide not only Ce^{+4} , but also Ce^{+3}, respectively [44], which indirectly indicates the presence of oxygen vacancies in cerium dioxide.

Based on the above, interaction of the PVA with the surface of CeO_2 can be represented following scheme (Fig. 7).

This interaction leads to the fact that the CeO_2 particles are located at a distance from each other and cannot coagulate [45].

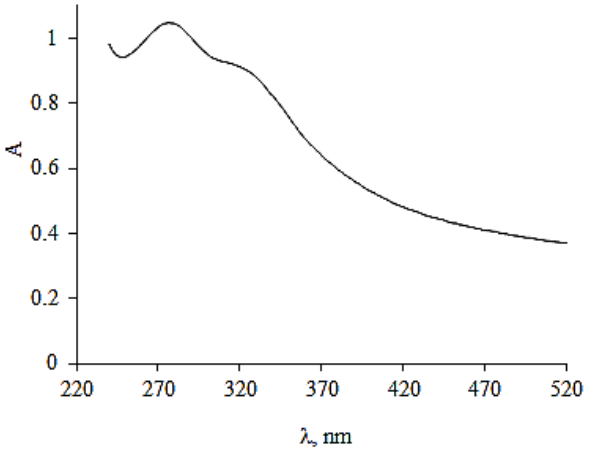

FIG. 6. UV absorption spectrum of sol CeO_2 with PVA

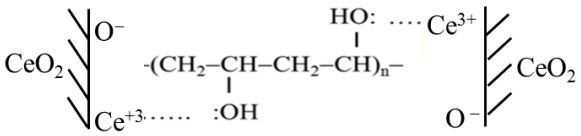

FIG. 7. Scheme of sorption PVA on the surface of colloidal CeO_2 particles

3.2. Photocatalytic, toxic and sunscreen properties sols

Before studying the photocatalytic activity of the samples (dried sol of CeO_2 with PVA and particles CeO_2 without PVA) under ultraviolet radiation, all samples were immersed in the setup reactor and kept in the dark for saturation adsorption. Equilibrium of adsorption was achieved after 60 min. Absorption capacity is possible due to oxygen vacancy defects on the surface of CeO_2, which is confirmed by UV spectroscopy and pH metric analysis. Photocatalytic destruction of an aqueous solution of MO under UV irradiation is shown in Fig. 8.

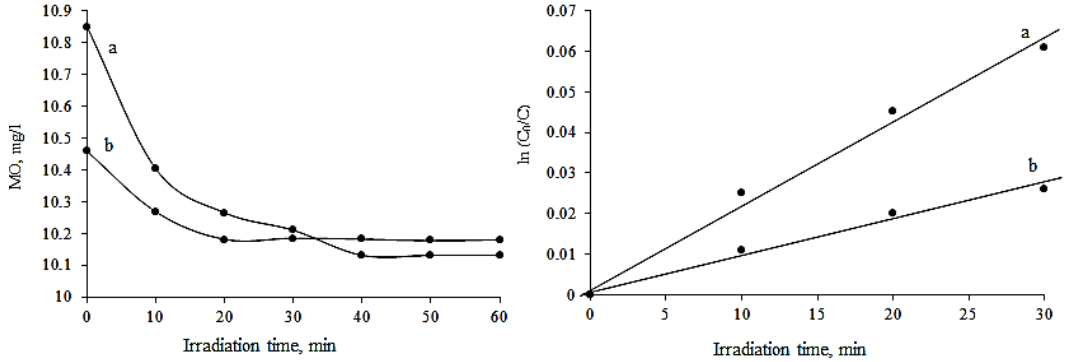

FIG. 8. Photocatalytic degradation of MO aqueous solution by sol CeO_2 with PVA (a) and particles CeO_2 without PVA under UV irradiation

The photocatalytic activity of the dried sol with PVA and particles CeO_2 without PVA obtained from the sol is very small. Fig. 8 shows that the presence of PVA reduces the sorption of MO on CeO_2 particles, but practically doesn't effect on the rate of photocatalysis and the degree of conversion of MO. The destruction of MO in the presence of a sample of CeO_2 with PVA occurs after 40 min and amounts to 6.2 %, and for the sample of CeO_2 without PVA – after 20 minutes is 2.6 %. An increase in the time of exposure to UV radiation (8 h) on the suspension does not lead to further decomposition of MO. Photodegradation reaction MO was adapted to the Langmuir–Hinshelwood model.

The slope of $\ln(C_0/C)$ plotted versus irradiation time (min) indicates the reaction rate constant of the sample. The rate constant of the reaction was measured as $2.2 \cdot 10^{-3}$ min^{-1} for sample with PVA and $0.9 \cdot 10^{-3}$ min^{-1} for sample without PVA. Small photocatalytic activity under UV irradiation is explained by recombination processes [46].

The sol of CeO_2 with PVA is characterized by the value of the critical wave absorption $\lambda_C = 353$ nm, which corresponds to "good" sunscreen properties on the classification of the FDA. Sol TiO_2 1 wt.% is characterized by $\lambda_C = 364$ nm and UVA/UVB = 0.36 [40]. The value of the UVA/UVB for sol CeO_2 with PVA is 0.64. Ultraviolet irradiation of the control areas of the exposed skin of rats for 10 minutes leads to the formation of ultraviolet erythema. Erythema intensity of 4 points is observed in all control areas of the skin with applied ointment base with PVA. After a day, the intensity of erythema drops to 3 points. Irradiation of the test sites applied with ointment base and fill with PVA/CeO_2 causes erythema intensity at 1 point. The absence of erythema (0 points) was observed at all experimental sites a day after irradiation. There were no cases of unscheduled death and complications in animals.

The results of the study of toxicity of sol CeO_2 with PVA and solid CeO_2 obtained from sol are show in Fig. 9. Fig. 9(a) shows, that the sol of CeO_2 with PVA inhibits the growth of the roots of Allium cepa. The results of microscopic examination of the roots of Allium cepa bulbs after their exposure in the sol of CeO_2 with PVA indicate a large number of heterochromatin clumps in the cell nuclei of the experimental samples. This feature is not anomalous, andmay indicate some genotoxic activity forthe sol. Fig. 9(b) shows that the optical density of samples after incubation of monocytes with solid CO_2 is significantly lower than that of intact cells. The average percentage of surviving lymphocytes was only 35.196 %. This indicates the cytotoxicity of cerium dioxide.

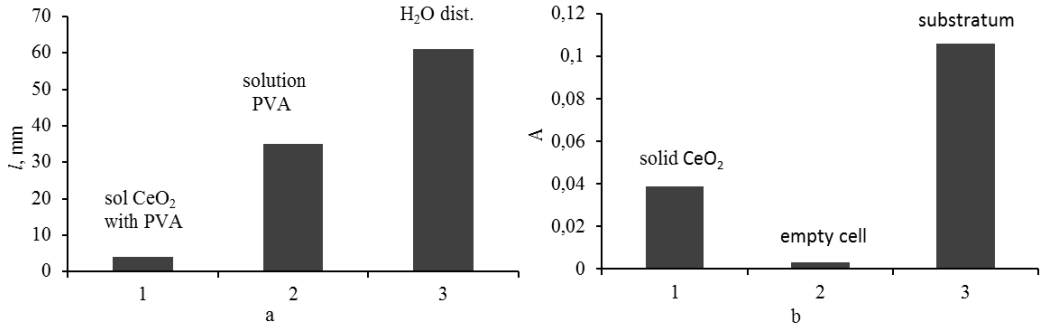

FIG. 9. Toxic properties of samples: the length of the roots of Allium cepa during exposure to samples (a), the optical density of the samples in the MTT test (b)

3.3. Conclusions

The CeO_2 sols stabilized by PVA 5 wt.% were obtained from solution of cerium nitrate (III) in the presence of hydrogen peroxide and different ammonia content. The sol remains stable at pH values ranging from 8.31 to 8.55. The size of colloidal particles in sols increases with increasing pH. The maximum size of the CeO_2 particles, which is not subjected to coagulation in the presence of 5 wt.% PVA is 67 ± 1 nm. The surface of cerium dioxide nanoparticles is characterized by acceptor properties due to the presence of Ce^{+3}. OH-groups of PVA are adsorbed onto the Ce^{+3} surface by a donor-acceptor mechanism. Interaction of PVA with the surface of CeO_2 nanoparticles prevents their agglomeration in the sol.

The sol of CeO_2 stabilized by with 5 wt.% PVA (pH = 8.55) has sun protection properties, which are not inferior to the properties of TiO_2 sols [5]. The sol in anointment base reduces the intensity of erythema in experimental animals irradiated with ultraviolet rays, while displaying low toxicity. The photocatalytic activity of this sol is weakly expressed.

References

[1] Paul J., Meechan C.W. Use of Ultraviolet Lights in Biological Safety Cabinets: A Contrarian View. *Appl. Bios.*, 2006, **11** (4), P. 222–227.

[2] Hirst S.M., Karakoti A.S., et al. Anti-inflammatory properties of cerium oxide nanoparticles. *Small*, 2009, **5** (24), P. 2848–2856.

[3] Bocca B., Caimi S., et al. ICP-MS based methods to characterize nanoparticles of TiO_2 and ZnO in sunscreens with focus on regulatory and safety issues. *Sci. Total. Environ.*, 2018, **630**, P. 922–930.

[4] Serpone N., Dondi D., Albini A. Inorganic and organic UV filters: Their role and efficacy in sunscreens and suncare products. *Inorg. Chem. Acta*, 2007, **360**, P. 794–802.

[5] Barbosa J.S., Neto D.M.A., et al. Ultrafast sonochemistry-based approach to coat TiO_2 commercial particles for sunscreen formulation. *Ultrason. Sonochem.*, 2018, **48**, P. 340–348.

[6] Bairi V.G., Lim J-H., Fong A., Linde Sean W. Size characterization of metal oxide nanoparticles in commercial sunscreen products. *J. Nanopart. Res.*, 2017, **19**, 256.

[7] Reinosa J.J., Docio C.M.Á., Ramírez V.Z., Lozano J.F.F. Hierarchical nano ZnO-micro TiO_2 composites: High UV protection yield lowering photodegradation in sunscreens. *Ceram. Int.*, 2018, **44** (3), P. 2827–2834.

[8] Kryczyk A., Zmudzki P., et al. The impact of ZnO and TiO_2 on the stability of clotrimazole under UVA irradiation: Identification of photocatalytic degradation products and in vitro cytotoxicity assessment. *J. Pharm. Biomed. Anal.*, 2017, **145**, P. 283–292.

[9] Shuwang D., Ling Z., et al. Controllable tartaric acid modified ZnO crystals and their modification determined optical, super hydrophilic/hydrophilic and photocatalytic properties. *J. Alloys Compd.*, 2018, **768**, P. 214–229.

[10] Gu Y., Wang L., et al. Study on Preparation and Functional Finishing of TiO_2 Supported Nano ZnO. *J. Nanosci. and Nanotech.*, 2018, **18** (11), P. 7703–7712.

[11] Wamer W.G., Yin J.J., Wei R.R. Oxidative damage to nucleic acids photosensitized by titanium dioxide. *Free Radical. Biol. Med.*, 1997, **23**, P. 851–858.

[12] Li R., Yabe S., et al. UV-shielding properties of zinc oxide-doped ceria fine powders derived via soft solution chemical routes. *Mat. Chem. Phys.*, 2002, **75**, P. 39–44.

[13] Li R., Yabe S., et al. Synthesis and UV-shielding properties of ZnO- and CaO-doped CeO_2 via soft solution chemical process. *Solid State Ionics*, 2002, **151**, P. 235–241.

[14] Yamashita M.., Kameyama K., et al. Synthesis and microstructure of calcia doped ceria as UV filters. *J. Mat. Sci.*, 2002, **37**, P. 683–687.

[15] Yabe S., Sato T. Cerium oxide for sunscreen cosmetics. *J. Solid State Chem.*, 2003, **171**, P. 7–11.

[16] Herrling T., Seifert M., Jung K. Cerium Dioxide: Future UV-filter in Sunscreen? *SOFW-Journal*, 2013, **139** (5), P. 11–14.

[17] Zholobak N.M., Ivanov V.K., et al. UV-shielding property, photocatalytic activity and photocytotoxicity of ceria colloid solutions. *J. Photochem. Photobiolog. B: Biology*, 2011, **102**, P. 32–38.

[18] Samai B., Chall S., Mati S.S., Bhattacharya S.C. Role of Silver Nanoclusters in the Enhanced Photocatalytic Activity of Cerium Oxide Nanoparticles. *Eur. J. Inorg. Chem.*, 2018, P. 3224–3231.

[19] Apostolescu N., Cernătescu C., et al. Promoting effect of ceria on the catalytic activity of CeO_2–ZnO polycrystalline materials. *Environ. Eng. and Manag. J.*, 2018, **17** (4), P. 765–770.

[20] Usharani S., Rajendran V. RTFM, RTPL and photocatalytic activity of CeO_2/ZrO_2 nanocomposites. *Chin. J. Phys.*, 2017, **55** (6), P. 2588–2596.

[21] Moongraksathum B., Chen Y. CeO_2-TiO_2 mixed oxide thin films with enhanced photocatalytic degradation of organic pollutants. *J. Sol-Gel Sci. Technol.*, 2017, **82**, P. 772–782.

[22] Fujita N., Kamada K. Protective effect of CeO_2 nanoparticles on photo-induced oxidative damage of DNA. *J. Ceram. Soc. Jpn.*, 2014, **122** (1422), P. 141–145.

[23] Laouedj N., Elaziouti A., Benhadria N., Bekka A. CeO_2 nanoscale particles: Synthesis, characterization and photocatalytic activity under UVA light irradiation. *J. Rare Earths.*, 2018, **36** (6), P. 575–587.

[24] Vatanparast M., Saedi L. Sonochemical-assisted synthesis and characterization of CeO_2 nanoparticles and its photocatalytic properties. *J. Mater. Sci. Mater. Electron.*, 2018, **29** (9), P. 7107–7113.

[25] Liu Zh., Li X., et al. Planar-dependent oxygen vacancy concentrations in photocatalytic CeO_2 nanoparticles. *Cryst. Eng. Comm.*, 2018, **20**, P. 204–212.

[26] Gao H., Yang H., Yang G., Wang Sh. Effects of oxygen vacancy and sintering temperature on the photoluminescence properties and photocatalytic activity of CeO_2 nanoparticles with high uniformity. *Mater. Technol.*, 2018, **33** (5), P. 321–332.

[27] Yuán S., Xu B., et al. Development of the visible?Light Response of $CeO_{2?x}$ with a high Ce^{3+} content and Its Photocatalytic Properties. *Chem. Cat. Chem.*, 2018, **10**, P. 1267–1271.

[28] So J-H., Oh M-H., Lee J-D., Yang S-M. Effects of Polyvinyl Alcohol on the Rheological Behavior and Phase Stability of Aqueous Silica Suspensions. *J. hem. ng. Jpn.*, 2001, **34** (2), P. 262–268.

[29] Dippon U., Pabst S., Klitzke S. Colloidal stabilization of CeO_2 nanomaterials with polyacrylic acid, polyvinyl alcohol or natural organic matter. *Sci. Tota. Environ.*, 2018, **645**, P. 1153–1158.

[30] Slizhov Y.G., Matveev T.N., Minakova T.S. Acid-base properties of the surface of chromatographic sorbents modified by metal acetylacetonates. *Russ. J. Phys. Chem. A*, 2012, **86** (3), P. 463–467.

[31] Jalava J., Taavitsaine V., Haario H., Lamberg L. Determination of particle and crystal size distribution from turbidity spectrum of TiO_2 pigments by means of t-matrix. *J. Quant. Spectrosc. Radiat. Transfer*, 1998, **60** (3), P. 399–409.

[32] Department of Health and Human Services. Food and Drug Administration. 21 CFR Parts 347 and 352 [WDocket No. 1978N0038] (formerly Docket No. 78N0038) RIN 0910AF43, Sunscreen Drug Products for Over-the-Counter Human Use; Proposed Amendment of Final Monograph, Federal Register. 2007, **72** (165), P. 49070–49122.

[33] Diffey B.L. A method for broad spectrum classification of sunscreens. *Int. J. Cosmet. Sci.*, 1994, **16**, P. 47–52.

[34] Guo Z., Zhou B., Sun W.L.X., Luo D. Hydrogen – rich saline protects against ultraviolet B radiation injury in rats. *J. Biomed. Res.*, 2012, **26** (5), P. 365–371.

[35] Davies E.K., Boyle Y., et al. Ultraviolet B-induced inflammation in the rat: A model of secondary hyperalgesia? *PAIN*, 2011, **152** (12), P. 2844–2851.

[36] Bishop T., Hewson D.W., et al. Characterisation of ultraviolet-B-induced inflammation as a model of hyperalgesia in the rat. *PAIN*, 2007, **131** (1–2), P. 70–82.

[37] Liman R., Acikbas Y., Ciğerci I.H. Cytotoxicity and genotoxicity of cerium oxide micro and nanoparticles by Allium and Comet tests. *Ecotoxicol. Environ. Saf.*, 2019, **168**, P. 408–414.

[38] Shishatskaya E.I., Dragana N., et al. Short-term culture of monocytes as an in vitro evaluation system for bionanomaterials designated for medical use. *Food Chem Toxicol.*, 2016, **96**, P. 302–308.

[39] Popov A.P., Priezzhev A.V., Lademann J., Myllyla R. TiO_2 nanoparticles as an effective UV-B radiation skin-protective compound in sunscreens. *J. Phys. D*, 2005, **38**, P. 2564–2570.

[40] Cross S.E., Innes B., et al. Human skin penetration of sunscreen nanoparticles: In-vitro assessment of a novel micronized zinc oxide formulation. *Skin. Pharmacol. Physiol.*, 2007, **20** (3), P. 148–154.

[41] Prosanov I.Y., Bulina N.V., Gerasimov K.B. Complexes of polyvinyl alcohol with insoluble inorganic compounds. *Phys. solid state*, 2013, **55** (10), P. 2132–2135.

[42] Prosanov I.Y., Matvienko A.A. Study of PVA thermal destruction by means of IR and RAMAN spectroscopy. *Phys. solid state*, 2010, **52** (10), P. 2203–2206.

[43] Tsunekawa S., Sivamohan R., et al. Structural study on monosize CeO_{2x} nano-particles. *Nanostruct. Mater.*, 1999, **11**, P. 141–147.

[44] Khalipova O.S., Kuznetsova S.A., Kozik V.V. Composition and properties of CeO_2–SiO_2 composite films prepared from film-forming solution. *Russ. J. Inorg. Chem.*, 2014, **59** (9), P. 913–917.

[45] Li Z., Aly Hassan A., Sahle-Demessie E., Sorial G.A. Transport of nanoparticles with dispersant through biofilm coated drinking water sand filters. *Water Res.*, 2013, **47**, P. 6457–6466.

[46] Saadat-Monfared A., Mohseni M. Polyurethane nanocomposite films containing nano-cerium oxide as UV absorber; Part 2: Structural and mechanical studies upon UV exposure. *Colloids Surfaces A*, 2014, **441**, P. 752–757.